

Monolithic total disc replacement made of polyurethane lattice based on anatomical features

Cite as: AIP Conference Proceedings **2537**, 020016 (2022); <https://doi.org/10.1063/5.0098589>
Published Online: 16 August 2022

Muhammad Hanif Nadhif, Joshua Yoshihiko Tampubolon, Muhammad Irsyad, et al.



View Online



Export Citation

ARTICLES YOU MAY BE INTERESTED IN

[Finite element analysis of C1 – L5 spinal bone simulators made of various high elastic modulus polymer filaments](#)

AIP Conference Proceedings **2537**, 020014 (2022); <https://doi.org/10.1063/5.0098411>

[Biocompatibility evaluation of bioabsorbable osteofixation devices: A scoping review](#)

AIP Conference Proceedings **2537**, 020008 (2022); <https://doi.org/10.1063/5.0098748>

[Possible molecular mechanisms of SARS-CoV-2 infection in saliva](#)

AIP Conference Proceedings **2537**, 030002 (2022); <https://doi.org/10.1063/5.0097978>



Time to get excited.

Lock-in Amplifiers – from DC to 8.5 GHz



[Find out more](#)


Zurich
Instruments

Monolithic Total Disc Replacement Made of Polyurethane Lattice based on Anatomical Features

Muhammad Hanif Nadhif^{1,2,a)}, Joshua Yoshihiko Tampubolon³, Muhammad Irsyad², Tri Kurniawati⁴, Ahmad Jabir Rahyussalim^{4,5,b)}

¹Medical Physics Department, Faculty of Medicine, Universitas Indonesia, DKI Jakarta 10430, Indonesia

²Medical Technology Cluster, Indonesia Medical Education and Research Institute (IMERI), Faculty of Medicine, Universitas Indonesia, DKI Jakarta 10430, Indonesia

³Biomedical Engineering Program, Department of Electrical Engineering, Faculty of Engineering, Universitas Indonesia, Depok 16424, Indonesia

⁴Stem Cells and Tissues Engineering (SCTE) Research Cluster, Indonesian Medical Education and Research Institute (IMERI), Faculty of Medicine, Universitas Indonesia, DKI Jakarta 10340, Indonesia

⁵Department of Orthopedics and Traumatology, Faculty of Medicine/Ciptomangunkusumo Central Hospital, Universitas Indonesia, DKI Jakarta 10430, Indonesia

Corresponding author: ^{b)}rahyussalim71@ui.ac.id, ^{a)}hanifnadhif@ui.ac.id

Abstract. Lower back pain (LBP) is included in the top 10 contributors to the overall disease burden. One of the etiologies of LBP is the intervertebral disc (IVD) degeneration, which in some cases, needs to be replaced with an artificial disc, the so-called total disc replacement (TDR). Unfortunately, TDR might provide post-surgical complications, including the failure in the metal-polymer assembly of TDR. The failure was argued due to the rigidity of the metal part and the shape of TDR that was not fully compliant with the anatomical features. Due to these complications, we proposed PU and monolithic construct to be alternative materials and comply with anatomical relevance. This study designed and developed a monolithic TDR made of PU lattices based on anatomical features. We focused on the IVDs in the lumbar section of the spine. The design step consisted of 3 phases: segmentation of DICOM files of IVDs using a 3D Slicer software, alignment using an Autodesk Meshmixer software, and lattice design using an Autodesk Inventor software. The manufacturing step started with a configuration setup in Simplify3D, software for computer-aided manufacturing (CAM) in 3D printing. The lattice features were fabricated using a Creality CP01 3D printer with two types of PU filaments: TPU 87A and TPU 95A. The printing results were able to construct the external curvature of the IVDs. Unfortunately, the microscopic measurement results showed that struts and holes' dimensions deviated from the design, which must be resolved in the next studies.

INTRODUCTION

Lower back pain (LBP) occurred in 1.4% to 20% out of the world population [1], which also increased with age [2]. LBP is one of the leading causes of disability that affects performance at work and general well-being [2–4], which contributes to more than 80 million disability-adjusted life years (DALYs) and the longest years lived with disability (YLD) of all conditions [5]. Among several indicative etiologies, intervertebral disc (IVD) degeneration in the lumbar section has been argued as the potential contributor to LBP [6,7].

Two advanced treatments for IVD degeneration problems are spinal fusion and intervertebral disc replacement (IDR). Unfortunately, spinal fusion has been reportedly reduced pelvic mobility, changed acetabular orientation, and possibly promoted pseudoarthrosis [8–10]. IDR, on the opposite, preserved the natural motion and spinal movement [6]. IDR can be formulated as total disc replacement (TDR) and nucleus pulposus replacement (NPR). The TDR mainly comprises two types of components: metallic and polymeric components. The metallic components were used to model the annulus fibrosus (AF) or to act as amounting to the intervertebral body, while the polymer part was

placed inside the AF-ish cage, reconstituting a nucleus pulposus (NP) [6]. On the other hand, NPR only replaces the NP part of the disc.

There are only three commercial TDR that was approved by the US Food and Drug Administration (FDA): Charité®, Maverick®, and activL® [11]. Nevertheless, studies about the use of TDR resulted in distinctive argumentations. Some reports elaborated upon the advantages of TDR over spinal fusion in the lumbar region [10,11]. However, a report stated that no differences were discovered between TDR and spinal fusion regarding the clinical relevance [12]. In addition, the report argued that the use of TDR should be limited at the research level until more proof appears [12]. Jacobs et al. (2013) [13] agreed with the argument, advising spine surgeons to be prudent when using the device in the future. Nonetheless, the significant challenge of using NPR was complications due to the swelling of hydrogels that may initiate gel fragmentation [14] and the detrimental impacts to the AF, regardless of the implant goals [15].

The limitations of both TDR and NPR trigger us to propose a monolithic construction of lumbar TDRs based on the biological counterparts' anatomical features. The monolithic TDR (MTDR) is made of thermoplastic polyurethane (TPU) due to its flexible properties, high tensile strengths, good resistance to non-polar fluids, excellent abrasion resistance, formability, and biocompatibility [16–18]. The MTDR is also featured with a lattice design to allow for both elasticity and toughness. In this study, we sought to develop the design and fabrication of an MTDR made of TPU that follows anatomical features of the real IVDs. Moreover, we also compared two types of TPU available in the market: TPU 87A and TPU 95A, which are distinguished by the chemical formula and hardness.

METHODS

Design

DICOM Segmentation

The lumbar vertebrae models were in the form of digital imaging, and communications in medicine (DICOM) files obtained from embodi3D (<https://www.embodi3d.com/files/file/39369-chest-ab-pelv-ct/>), a platform for the biomedical 3D printing community. The DICOM files were segmented using a 3D Slicer software with five sequential steps: 1) lumbar section crop (Fig. 1a), 2) mask volume segmentation (Fig. 1b), 3) detailed segmentation of L1-L5 vertebral bodies (Fig. 1c), 4) detailed segmentation of L1-L5 IVD models (Fig. 1d), and 5) data export to an .stl format.

For the lumbar section crop, the DICOM files were imported to a 3D Slicer software by choosing the load data button on the interface. On the module options, chose volume rendering. After that, click the volume input and decided the region of interest (ROI). The ROI can be manually dragged from slices or from the advance bar. To better view the bony structure, the display for the DICOM active volume was set to grey and interpolated with details: 1) threshold: -1,000 to 1,000, 2) W: 589, and 3) L: 425. The volume rendering in this study used the preset of CT-AAA with zero shift.

In the volume segmentation, the whole chunk of the body was taken since the ROI is in the form of a box. Subsequently, the volume was isolated to facilitate the perspective-shifting if required. Next, the volume was cropped using the threshold with a range of 63.16 – 1125.00 so that only the vertebral volume was included while other surrounding tissues were removed. The next step was manually removing every artifact from the isolated volume using a scissor effect and erase for 3D removal and detailed removal in each slice, respectively. The mask volume was chosen to remove every bit and make a new volume comprising only the lumbar section. To make the mask volume transparent, filler outside the mask volume was set to -10,000.

The masking of previous segmentation can be used further to extract the vertebral bodies. The use of scissors, eraser and paint effect enhanced the visibility of the segments. The three tools in 3D Slicer were also important to separate the joined segments from the nearby cartilages. The detailed segmentation of L1-L5 vertebral bodies was performed on Mahadevan to provide accurate results [7]. The cleaning process was done per slice from the three perspectives, started from the sagittal and coronal views and finalized with the axial view.

The detailed segmentation of L1-L5 IVDs referred to the work of Khan et al. [19]. In 3D slicer, the volume modulus was set using two parameters: PET color scheme (W: 1,238, L: -1,461) and threshold (-11,113 – 2,238). Next, the blanks inside the vertebrae were filled, while the segment editor module was used to manually paint the voxel on the cavity, hence annotating the IVDs.

The annotated IVDs were exported from 3D Slicer as standard tessellation (.stl) files. The export was started by clicking the segment editor module and continued by clicking the segmentation sections. Afterward, the export option was selected, and the desired conditions were input on the files.

Alignment

The stl files of the IVDs were imported into an Autodesk Meshmixer design software. The first thing to do was clicking on the edit module and choosing alignment to set up the source and destination. This project chooses the base point and World Origin/Y-Up. After that click, the alignment was finished, and the files were exported with an stl format for the lattice design.

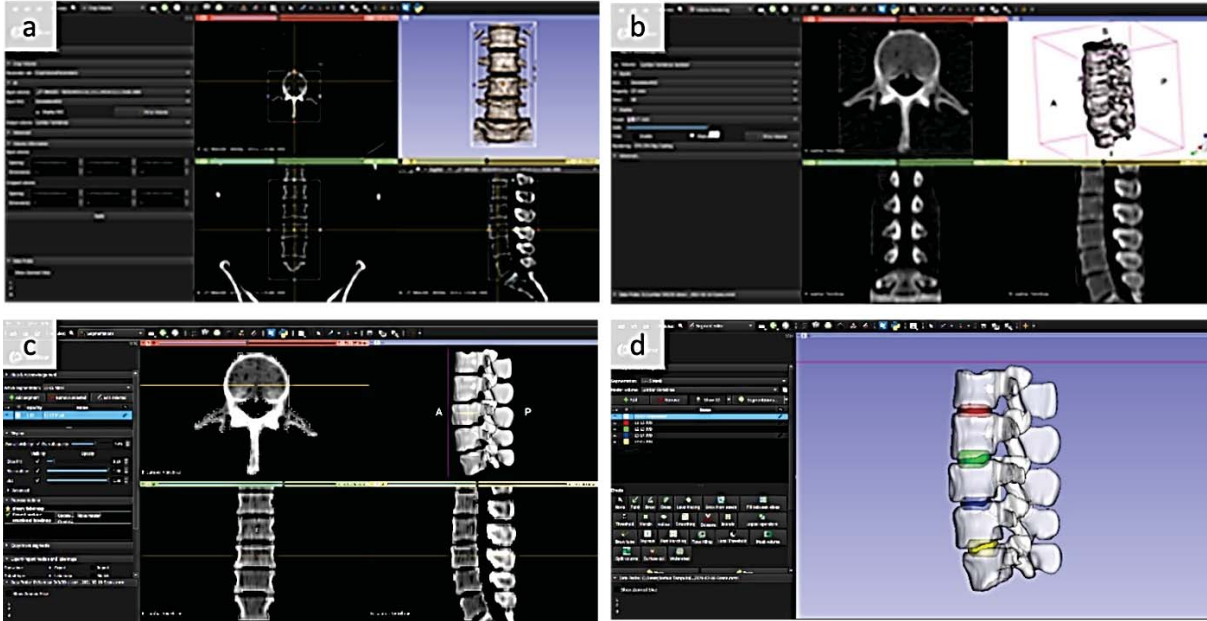


FIGURE 1. Screenshots of lumbar section crop (a), mask volume segmentation (b), detailed segmentation of L1-L5 vertebral bodies (c), and detailed segmentation of L1-L5 IVD models (d).

Lattice Design

The lattice design was performed using Autodesk Inventor design software. The lattice design followed the works of Christiani et al. [20]. The strut width and thickness were 0.7 mm and 1.0 mm, respectively. The hole between each strut was 1.3 mm. The strut layers were oriented at the angle (θ) of 30° from the horizontal line. After finishing the lattice design, the files were saved in a .stl format.

Fabrication

Computer-Aided Manufacturing (CAM)

Before the MTDRs were fabricated by means of 3D printing, the printing parameters were configured in Simplify 3D CAM software [21]. The CAM process started with the import of the stl files. Unlike the usual 3D printing setup that forms top solid layers, bottom solid layers, and outline shells, the 3D printing in this study did not build the three features to produce an open lattice configuration, thereby generating a porous MTDR. The printing parameters were set as presented in Table 1.

TABLE 1. 3D printing parameters

| Simplify 3D Parameter | Value |
|------------------------------|--------------|
| Extrusion width (mm) | 0.35 |
| Extrusion multiplier | 1.1 |
| Layer height (mm) | 0.1 |
| Infill percentage (%) | 100 |
| Printing speed (mm/s) | 30 |
| Outline overlap (%) | 15 |
| Nozzle temperature (°C) | 210 |
| Bed temperature (°C) | 70 |

3D Printing Setup

The 3D printing used to fabricate MTDRs was a CP-01 3D printer from Creality 3D Technology Co., Ltd. (Shenzhen, China) [21]. The printer uses the fused deposition modeling (FDM) principle and is equipped with two stepper motors connected with lead screws to actuate movements in the vertical axis (z-axis). In the horizontal plane, the other two axes are linked up with belts to actuate movements in the x- and y- axes. The 3D printing filament is extruded using a stepper motor. The 3D printing nozzle has a diameter of 0.4 mm, allowing for the selected extrusion width in Simplify3D.

This study used two types of thermoplastic polyurethane (TPU) filaments: TPU 87A and TPU 95A (eSun Industrial Co., Ltd., Shenzhen, China). TPU 87A is made of pure polyurethane, whereas TPU 95A contains adipic acid (50%), methacrylamide (30%), and 2,3-butanediol (20%). The XA (i.e., 87A and 95A) code demonstrates the shore hardness of the material, and the higher number means the higher hardness.

Measurement & Statistical Analysis

After every MTDR was fabricated, the struts and holes in the lattice construction were measured using a Dinolite microscope camera. Each sample's struts and holes were measured randomly in ten different locations to calculate the average strut and hole widths for each sample. The standard deviation (SD) of the struts and holes were also examined to identify the printing consistency. The measured struts and holes were subsequently compared with the setpoints to determine the errors, resulting in the root mean square error (RMSE). All the mentioned statistical analyses were performed in Python with several modules: NumPy, Seaborn, Pandas, and Scikit-learn.

RESULTS & DISCUSSION

Design

The DICOM segmentation processes produced 3D models of IVDs at L1/L2 (Fig. 2a), L2/L3 (Fig. 2b), L3/L4 (Fig. 2c), and L4/L5 (Fig. 2d) IVDs. The four models of IVDs were subsequently aligned using MeshMixer. The example of the alignment result is presented in Fig. 2e. After alignment, lattice features were applied in Inventor. The top view of one of the IVD models is shown in Fig. 2f.

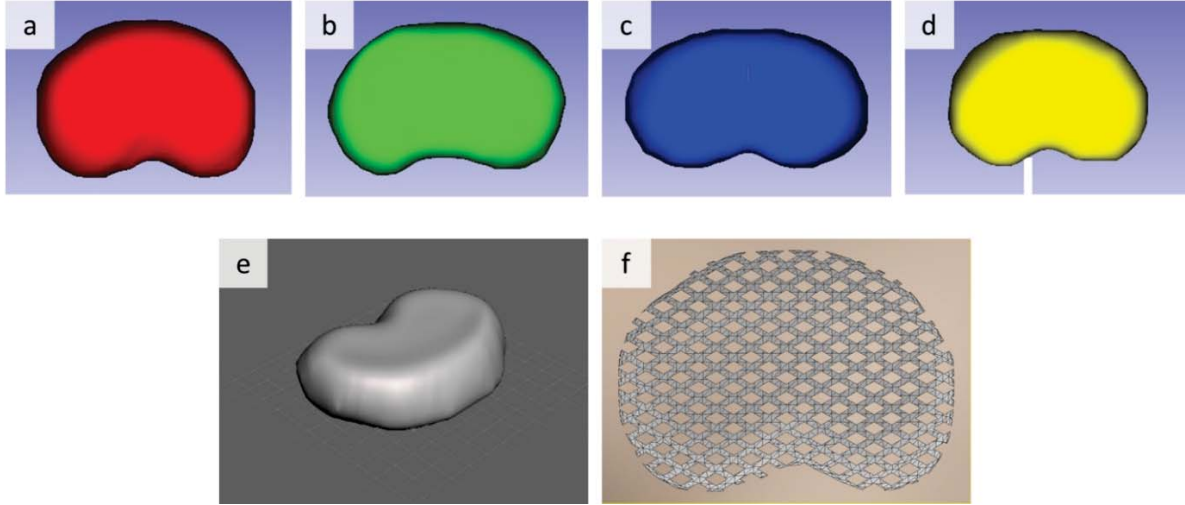


FIGURE 2. IVD Models of L1/L2 (a), L2/L3 (b), L3/L4 (c), and L4/L5 (d); an example of alignment results using MeshMixer (e); a top view example of the lattice design in an IVD model (f)

Fabrication

Monolithic TDRs for the lumbar region was successfully 3D printed with two materials: TPU 87A and TPU 95A. The photographs of the TDRs from the two materials are presented in Fig. 3: the top row for TPU 87A and the bottom row for TPU 95A.

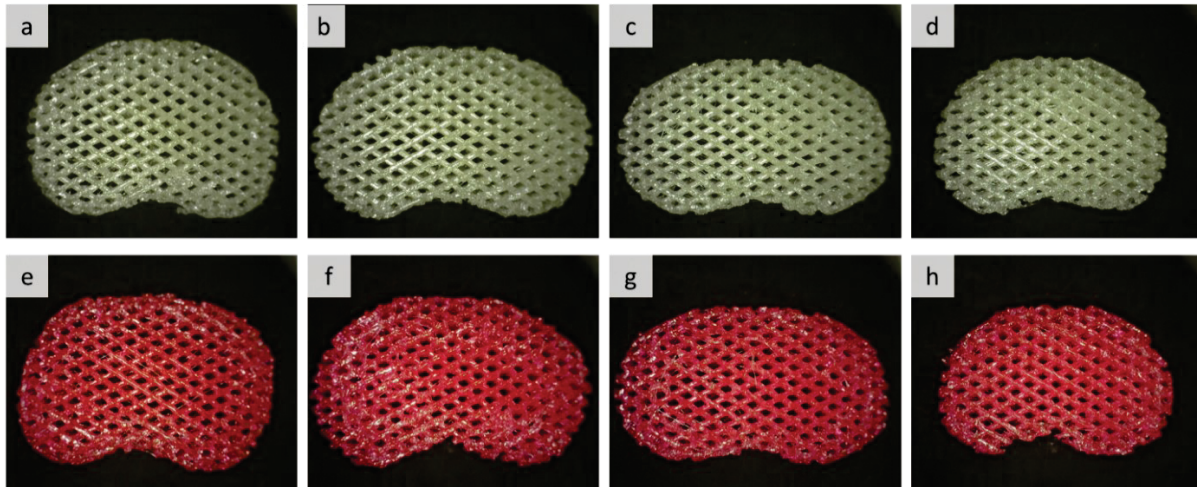


FIGURE 3. Top views of MTDRs made of TPU 87A (L1-L2 (a), L2-L3 (b), L3-L4 (c), and L4-L5(d)) and TPU 95A (L1-L2 (e), L2-L3 (f), L3-L4 (g), and L4-L5(h)).

Measurement

The measurement result is presented in Table 2 and Fig. 4. The widths of struts and holes for the two materials were similar for each IVD. The average strut widths for TPU 87A and 95A were 0.84 mm and 0.85 mm, respectively. Meanwhile, the average hole widths for TPU 87A and 95A were 1.04 mm and 1.05 mm, respectively. The printing of the two materials was arguably consistent, indicated by the small deviation. The highest standard deviation was 0.18 mm for both TPU 87A-L1L2 and TPU 87A-L3L4. For overall results, the struts were more consistent than the holes,

indicated by smaller standard deviation values. When comparing the two materials, the standard deviation of TPU 87A was smaller than 95A.

Unfortunately, the overall RMSEs for strut and hole widths were relatively high. For TPU 87A and 95A, the RMSEs for the hole were 0.30 mm and 0.32 mm, respectively. These values were higher than for the strut, for which RMSEs were 0.16 mm and 0.18 for TPU 87A and 95A, respectively. Similar to the standard deviation results, the RMSE of TPU 87A was lower than of TPU 95A. For struts, the smallest RMSE was 0.12 mm, while the highest RMSE was 0.21 mm. On the other hand, the minimum and the maximum RMSEs for holes were 0.22 mm and 0.38, respectively. The errors in the design were undesirable. For future studies, the deviated results from the design can potentially be minimized by tuning the printing parameters. The tuning for the strut-hole configuration was not extensively conducted since this study's main goal was to emphasize the anatomical reconstitution of IVD outer curvatures in the MTDR.

The smaller values of standard deviation and RMSE for TPU 87A were interesting to discover, meaning that the printing of TPU 87A is more accurate and precise than TPU 95A. Hypothetically speaking, the result difference between the two materials was mainly due to the printing parameters. We argue that the printing parameters for the two materials should be distinguished by tuning and optimization. However, as mentioned earlier, the tuning and optimization were outside the limit of this study.

TABLE 2. 3D Printing Parameters

| Component | Filament | MTDR | Mean (mm) | St. Dev (± mm) | RMSE (mm) | Mean (mm) | St. Dev. (± mm) | RMSE (mm) |
|-----------|----------|------|-----------|----------------|-----------|-----------|-----------------|-----------|
| TPU 87A | Struts | L1L2 | 0.80 | 0.06 | 0.12 | 0.84 | 0.08 | 0.16 |
| | | L2L3 | 0.85 | 0.07 | 0.16 | | | |
| | | L3L4 | 0.83 | 0.05 | 0.14 | | | |
| | | L4L5 | 0.88 | 0.11 | 0.21 | | | |
| | Holes | L1L2 | 0.99 | 0.13 | 0.33 | 1.04 | 0.14 | 0.30 |
| | | L2L3 | 1.05 | 0.16 | 0.30 | | | |
| | | L3L4 | 1.09 | 0.08 | 0.22 | | | |
| | | L4L5 | 1.03 | 0.15 | 0.31 | | | |
| TPU 95A | Struts | L1L2 | 0.81 | 0.13 | 0.18 | 0.85 | 0.10 | 0.18 |
| | | L2L3 | 0.87 | 0.07 | 0.18 | | | |
| | | L3L4 | 0.84 | 0.10 | 0.17 | | | |
| | | L4L5 | 0.88 | 0.08 | 0.20 | | | |
| | Holes | L1L2 | 0.96 | 0.18 | 0.38 | 1.02 | 0.15 | 0.32 |
| | | L2L3 | 1.04 | 0.12 | 0.28 | | | |
| | | L3L4 | 1.01 | 0.18 | 0.34 | | | |
| | | L4L5 | 1.08 | 0.10 | 0.24 | | | |

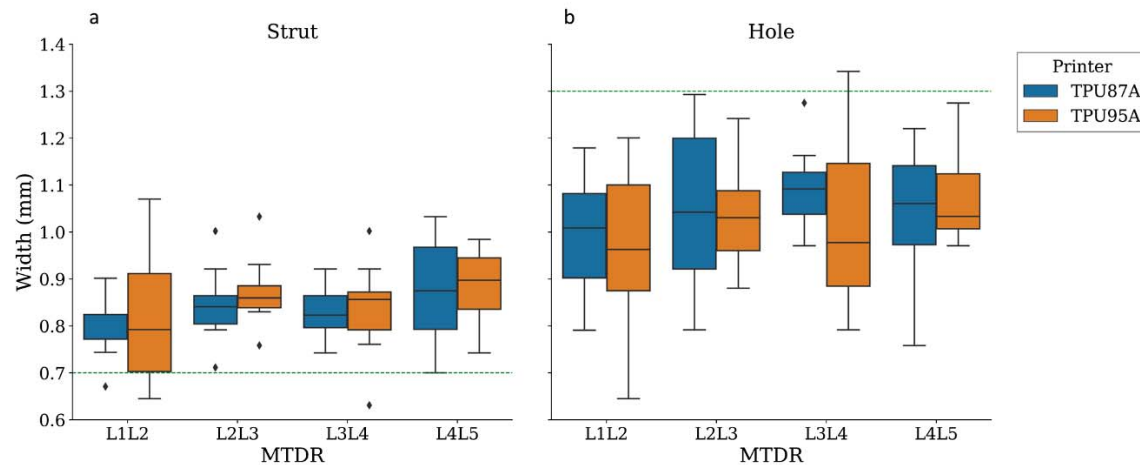


FIGURE 4. Widths of struts (a) and holes (b) for each MTDR

CONCLUSION

Anatomical compliant MTDRs made of TPU have been successfully designed and fabricated. The design was made feasible through three steps: DICOM segmentation, alignment, and lattice design. Meanwhile, MTDRs have been successfully produced by FDM with accurate modeling of the outer curvature of the lumbar IVDs. Overall, TPU 87A and TPU 95A provided good printing results of the lattice architecture. Unfortunately, the errors between the design setpoints and the resulted struts and holes were still relatively high. These issues need to be resolved in the future by tuning in the printing parameters. For further development of the MTDRs, it is of importance to perform a biocompatibility study of the products so that they can be followed up to clinical trials and finally to commercialization.

ACKNOWLEDGMENT

This research was supported by the Universitas Indonesia PUTI 2020 Grant from Universitas Indonesia with Contract Number NKB-888/UN2.RST/HKP.05.00/2020.

REFERENCES

1. F. Fatoye, T. Gebrye, and I. Odeyemi, *Rheumatol Int* **39**, 619 (2019).
2. A. Wu, L. March, X. Zheng, J. Huang, X. Wang, J. Zhao, F.M. Blyth, E. Smith, R. Buchbinder, and D. Hoy, *Ann Transl Med* **8**, 299 (2020).
3. W. Kaplan, V.J. Wirtz, A. Mantel-Teeuwisse, P. Stolk, B. Duthey, and R. Laing, *Priority Medicines for Europe and the World 2013 Update* (World Health Organization in collaboration with Utrecht University and Boston University, Geneva, 2013).
4. R. Buchbinder, F.M. Blyth, L.M. March, P. Brooks, A.D. Woolf, and D.G. Hoy, *Best Practice & Research Clinical Rheumatology* **27**, 575 (2013).
5. N. Henschke, S.J. Kamper, and C.G. Maher, *Mayo Clinic Proceedings* **90**, 139 (2015).
6. B.R. Whatley and X. Wen, *Materials Science and Engineering: C* **32**, 61 (2012).
7. A. Malandrino, J. Noailly, and D. Lacroix, *PLoS Comput Biol* **7**, e1002112 (2011).
8. J. Bernstein, R. Charette, M. Sloan, and G.-C. Lee, *Clin Orthop Relat Res* **477**, 324 (2019).
9. E. Ebrahimzadeh, *Clin Orthop Relat Res* **477**, 331 (2019).
10. J. Zigler, M.F. Gornet, N. Ferko, C. Cameron, F.W. Schranck, and L. Patel, *Global Spine Journal* **8**, 413 (2018).
11. J.J. Yue, R. Garcia, and L.E. Miller, *Med Devices (Auckl)* **9**, 75 (2016).
12. K.D. van den Eerenbeemt, R.W. Ostelo, B.J. van Royen, W.C. Peul, and M.W. van Tulder, *Eur Spine J* **19**, 1262 (2010).
13. W.C.H. Jacobs, N.A. van der Gaag, M.C. Kruyt, A. Tuschel, M. de Kleuver, W.C. Peul, A.J. Verbout, and F.C. Oner, *Spine* **38**, 24 (2013).
14. E. Durdag, O. Ayden, S. Albayrak, I.B. Atci, and E. Armagan, *Turk Neurosurg* **24**, 602 (2014).
15. G.W. Omlor, A.G. Nerlich, H. Lorenz, T. Bruckner, W. Richter, M. Pfeiffer, and T. Gühring, *Eur Spine J* **21**, 1700 (2012).
16. H. Lee, R. Eom, and Y. Lee, *Advances in Materials Science and Engineering* **2019**, 1 (2019).
17. N. Gama, A. Ferreira, and A. Barros-Timmons, *J Polym Environ* **28**, 1560 (2020).
18. M.H. Nadhif, M. Irsyad, M. Satrio, M. Suhaeri, and Y. Whulanza, *Journal of Mechanical Engineering* **18**, 11 (2021).
19. A.N. Khan, H.E. Jacobsen, J. Khan, C.G. Filippi, M. Levine, R.A. Lehman, K.D. Riew, L.G. Lenke, and N.O. Chahine, *Ann. N.Y. Acad. Sci.* **1410**, 68 (2017).
20. T.R. Christiani, E. Baroncini, J. Stanzone, and A.J. Vernengo, *Regenerative Biomaterials* **6**, 175 (2019).
21. M. Nadhif, M. Irsyad, A. Rahyussalim, and M. Utomo, in *Proceedings of The 4th International Seminar on Metallurgy and Materials* (AIP, Jakarta, Indonesia, 2021), p. 030006.